

# TRM versus FRP in flexural strengthening of RC beams: Behaviour at high temperatures



Saad M. Raouf<sup>a,b,\*</sup>, Dionysios A. Bournas<sup>c</sup>

<sup>a</sup> Department of Civil Engineering, University of Nottingham, NG7 2RD Nottingham, UK

<sup>b</sup> Department of Civil Engineering, University of Tikrit, Tikrit, Iraq

<sup>c</sup> European Commission, Joint Research Centre (JRC), Directorate for Space, Security and Migration, Safety and Security of Buildings Unit, via E. Fermi 2749, I-21027 Ispra, Italy

## ARTICLE INFO

### Article history:

Received 28 May 2017

Accepted 21 July 2017

### Keywords:

Reinforced concrete  
Textile reinforced mortar  
TRM  
High temperature  
Strengthening  
FRCM  
TRC  
Carbon fibre  
Basalt fibre  
Glass fibres  
Debonding

## ABSTRACT

The flexural behaviour of RC beams strengthened with TRM and FRP composites was experimentally investigated and compared both at ambient and high temperatures. The investigated parameters were: (a) the strengthening material, namely TRM versus FRP, (b) the number of strengthening layers, (c) the textile surface condition (dry and coated), (d) the textile material (carbon, basalt or glass fibres) and (e) the end-anchorage of the flexural reinforcement. A total of 23 half-scale beams were constructed, strengthened in flexure and tested to assess these parameters and the effectiveness of the TRM versus FRP at high temperatures. TRM exhibited excellent performance as strengthening material in increasing the flexural capacity at high temperature; in fact, TRM maintained an average effectiveness of 55%, compared to its effectiveness at ambient temperature, contrary to FRP which totally lost its effectiveness when subjected to high temperature. In specific, from the high temperature test it was found that by increasing the number of layers, the TRM effectiveness was considerably enhanced and the failure mode was altered; coating enhanced the TRM effectiveness; and the end-anchorage at high temperature improved significantly the FRP and marginally the TRM effectiveness. Finally, the formula proposed by the *fib* Model Code 2010 was used to predict the mean debonding stress in the TRM reinforcement, and using the experimental results obtained in this study, a reduction factor to account for the effect of high temperature on the flexural strengthening with TRM was proposed.

© 2017 The Authors. Published by Elsevier Ltd. This is an open access article under the CC BY license (<http://creativecommons.org/licenses/by/4.0/>).

## 1. Introduction and background

Due to the continuous deterioration of RC structures, both in seismic and non-seismic areas, the need for upgrading the existing concrete structures has become very important. Ageing, degradation due to environmental conditions, inadequate maintenance, increase of applied permanent or earthquake loads, and the need to meet the requirements of modern design codes (i.e. Eurocodes) are the main reasons which advocate for the urgent need of structural strengthening the existing RC structures. The use of Fibre Reinforced Polymer (FRP) as a means of external reinforcement for RC structures has gained popularity due to the favorable properties of FRP such as the high strength to weight ratio, ease and speed of application, resistance to corrosion, and minimal change in the geometry of structural

elements. Nevertheless, FRP has some disadvantages such as high costs, incompatibility with concrete surfaces, difficulty to apply on wet surfaces or low temperatures, and poor performance at high temperature. The latter is due to epoxy resins used in FRP which lose their tensile capacity under high temperature. Therefore, unless protective (thermal insulation) systems are provided [1], the effectiveness of TRM will be extremely low due to the deterioration of bond at the concrete-adhesive interface when the interface temperature is above the glass transition temperature ( $T_g$ ). A state-of-the-art review on the fire performance of reinforced concrete (RC) members strengthened with FRP and subjected to fire and high temperatures was recently presented by Firmo et al. 2015 [2].

In an attempt to overcome such drawbacks, a new generation of composites combining high strength textile fibres with inorganic matrices have been recently proposed as a structural retrofitting material for the deficient RC members namely the textile reinforced mortar (TRM) [3], identified in the literature also as TRC [4] or FRCM [5]. In comparison with FRP, TRM is a relatively low cost strengthening material, safer for manual workers, compatible

\* Corresponding author at: Department of Civil Engineering, University of Nottingham, NG7 2RD Nottingham, UK.

E-mail addresses: [Saad.Raouf@nottingham.ac.uk](mailto:Saad.Raouf@nottingham.ac.uk), [Dionysios.BOURNAS@ec.europa.eu](mailto:Dionysios.BOURNAS@ec.europa.eu) (S.M. Raouf), [Dionysios.BOURNAS@ec.europa.eu](mailto:Dionysios.BOURNAS@ec.europa.eu) (D.A. Bournas).

with concrete and masonry substrates and can be applied on wet surfaces or at low temperatures.

Bond between TRM and concrete substrate has been addressed in several studies [i.e. 6,7]. TRM has also been investigated as a means of external reinforcement for strengthening RC members, namely in flexural reinforcing of RC beams [i.e. 8–11], one way [12,13], and two way slabs [14,15]; the shear upgrading of RC elements [i.e. 16–20]; the seismic retrofitting of RC columns [21–26]; and the seismic reinforcing of infilled RC frames [27]. The experimental results demonstrated the effectiveness of TRM as a retrofitting solution. TRM has been successfully used worldwide in the construction field. Selected case studies can be found in [28].

TRM could outperform FRP systems at high temperatures or fire due to the breathability, non-combustibility, and non-flammability offered by mineral-based cement mortars used as binding materials. In general, the research on the performance of TRM systems at high temperature or fire and the comparison between TRM and FRP systems at high temperature or fire is extremely limited [29–33]. This is attributed to the experimental difficulties associated with applying simultaneously loading and high temperatures. For this reason, the past studies were mainly focused on evaluating the residual strength of TRM after being exposed to high temperatures and cooled down. Particularly, in [29–31] uniaxial tensile tests were conducted on TRM coupons made of glass [29], carbon [30], and basalt [31] textile fibres. The specimens were exposed to different level of high temperature varied between 20 and 1000 °C, cooled down and then subject to tensile loading up to failure. The main conclusion of these studies was that the TRM coupons maintained their ambient tensile strength up to 200 °C [29,30], and 150 °C [31], but for higher temperatures the residual tensile strength was gradually decreased.

The only studies reported in the literature on the effectiveness of TRM versus FRP as strengthening materials at high temperature are those of Raouf and Bournas 2017 [34], Tetta and Bournas 2016 [35], and Bisby et al. 2013 [36].

In [34] the authors investigated the bond behaviour between TRM vs. FRP and concrete at high temperatures, whereas [35] studied the effectiveness of TRM vs. FRP in shear strengthening of concrete members subjected to high temperatures. In both studies, specimens were heated up to predefined temperatures equal to 20, 50, 75, 100, 150, 300, 400 and 500 °C in [34] and 20, 100, 150 and 250 °C in [35], and then subjected to double-lap shear test [34] and three point-bending test [35], demonstrating superior performance for TRM over FRP at high temperature. In particular, in [34], it was found that TRM specimens maintained an average of 85% of their ambient bond strength up to 400 °C, contrary to FRP which kept only 17% at 150 °C. Similarly, in [35] it was shown that TRM maintained 60% of its ambient temperature shear strengthening effectiveness at 150 °C, contrary to FRP which totally lost its effectiveness when subjected to temperature above the  $T_g$ .

Finally, in [36], FRP and TRM flexurally retrofitted beams were subjected to a sustained load and then exposed to increasing temperature up to failure, keeping however the end anchorage TRM and FRP zones cold. It was concluded that both TRM and FRP can have the same performance at high temperature when their anchorage is kept cold. However, in that study, the effect of high temperature on the FRP/TRM debonding mechanism was not addressed because the bond condition was not realistically simulated due the cold anchorage zones.

From the literature survey, it is clear that the subject of TRM vs. FRP in flexural strengthening of RC beams subjected to high temperature has not covered and needs to be studied in realistic bond conditions for the externally bonded reinforcement. This paper investigates for the first time the effectiveness of TRM vs. FRP in flexural strengthening of RC beams subjected to simultaneous high temperature and loading, without protecting the TRM and FRP

anchorage zones. The parameters investigated include the number of FRP/TRM layers (1, 3, and 7), the textile surface condition (dry and coated), the textile fibre materials (carbon, basalt, and glass), and the end-anchorage system of the flexural reinforcement.

## 2. Experimental programme

### 2.1. Test specimens and investigated parameters

The main objective of the current study was to compare the performance of TRM versus FRP in enhancing the flexural capacity of RC beams at high temperature. A total of 23 half-scale rectangular section RC beams (dimensions of 101 × 202 mm) were constructed, strengthened and tested under 4-point bending load. The total length of the beams was 1675 mm, whereas the effective and shear span were 1500 mm, 580 mm, respectively (Fig. 1a).

All beams were intentionally designed with a low amount of longitudinal reinforcement so as to have low flexural capacity. The reinforcement ratio ( $\rho_s$ ) was equal to 0.56%, simulating flexural-deficient beams as a result of corrosion of rebars or increase of the applied load. As shown in Fig. 1b, the longitudinal reinforcement comprised two 8 mm diameter rebars at the bottom (tension zone) and two 12 mm diameter deformed rebars at the top (compression zone) of the beams. The tensile rebars were bent at their ends over 180 degrees to provide proper anchorage. As shown in Fig. 1a, 8 mm-diameter shear links were placed at 80 mm distances along the two clear shear spans of the beams (expect for the constant moment zone) resulting – by design – to a shear resistance seven times higher than the shear force corresponding to the predicted flexural capacity of the unstrengthened beam.

Several parameters were investigated in this study including: (a) the strengthening system (TRM versus FRP), (b) the number of strengthening layers (one, three, and seven), (c) the material of the textiles fibres (carbon, glass and basalt), (d) the textile surface condition (coated versus dry) of carbon-fibre textiles, and (e) the end-anchorage of the main FRP/TRM reinforcement using 2-layers U-shaped jacketing made of FRP/TRM. All these parameters were investigated at ambient (20 °C) and high (150 °C) temperatures.

Table 1 supporting by Fig. 2a, provide description of the tested specimens and strengthening configurations. The strengthened specimens were named following the notation BN\_F\_T, where B denotes the type of bonding agent (M for cement mortar and R for epoxy resin); N the number of TRM or FRP layers; F the type of textile fibres material (C for dry carbon fibres, CCo for coated carbon fibres, BCo for basalt fibres and G for glass fibres); and T denotes the temperature at which the specimens were exposed (20 °C or 150 °C). For the specimens receiving U-jackets at their ends (Fig. 2b), an additional suffix (EA-End anchorage) is added to the notation. For example, 'M3\_C\_20' refers to a beam strengthened with 3 layers of dry carbon TRM and tested at 20 °C, whereas 'R3\_C\_EA\_150' refers to a beam strengthened with 3 layers of carbon FRP, anchored at its ends using two layers of U-shaped jacket, and tested at temperature of 150 °C. It is noted that the axial stiffness of seven layers of glass or basalt-fibre textile are approximately equivalent to one layer of carbon-fibre textile. Table 1 gives the normalized axial stiffness of the textile reinforcement used in all specimens (normalized to one layer of carbon-fibre textile).

### 2.2. Materials and strengthening procedure

The beams were cast in four different groups using the same concrete mix-design. The concrete compressive and splitting

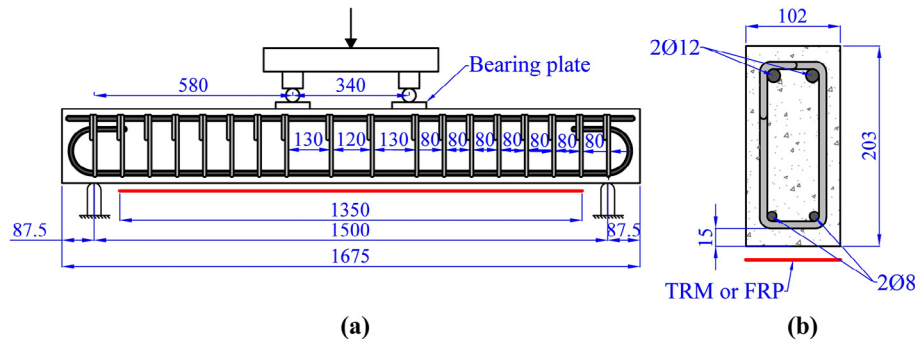


Fig. 1. Details of test beams: (a) Beam geometry and reinforcement; (b) cross section (dimensions in mm).

**Table 1**  
Strengthening configuration and materials properties of test specimens.

Specimen	$t^*$ (mm)	No. of layers	Ratio of axial stiffness <sup>**</sup>	$\rho_f^{***}$ (%)	Temperature (°C)	Concrete Strength (MPa)		Mortar Strength (MPa)	
						Compressive strength <sup>†</sup>	Tensile splitting strength <sup>†</sup>	Compressive strength <sup>†</sup>	Flexural strength (MPa)
CON	–	–	–	–	20	19.9 (0.5)	2.1 (0.06) <sup>†</sup>	–	–
<i>TRM-retrofitted</i>									
M1_C_20 <sup>1</sup>	0.095	1	1	0.0475	20	19.9 (0.5)	2.1 (0.06)	39.2 (1.7)	9.8 (0.6)
M1_C_150 <sup>1</sup>	0.095	1	1	0.0475	150	20.7 (1.1)	1.9 (0.09)	16.2 (0.9)	2.3 (0.2)
M1_CCo_20 <sup>1</sup>	0.095	1	1	0.0475	20	19.9 (0.5)	2.1 (0.06)	39.2 (1.8)	9.8 (0.6)
M1_CCo_150	0.095	1	1	0.0475	150	20.7 (1.1)	1.9 (0.09)	16.2 (0.9)	2.3 (0.2)
M3_C_20 <sup>1</sup>	0.095	3	3	0.1425	20	19.9 (0.5)	2.1 (0.06)	39.2 (1.9)	9.8 (0.6)
M3_C_150	0.095	3	3	0.1425	150	20.7 (1.1)	1.9 (0.09)	16.2 (0.9)	2.3 (0.2)
M7_BCo_20 <sup>1</sup>	0.0371	7	1.06	0.1299	20	19.9 (0.5)	2.1 (0.06)	39.2 (1.7)	9.8 (0.6)
M7_BCo_150	0.0371	7	1.06	0.1299	150	20.7 (1.1)	1.9 (0.09)	16.2 (0.9)	2.3 (0.2)
M7_G_20 <sup>1</sup>	0.044	7	1.07	0.1540	20	19.9 (0.5)	2.1 (0.06)	39.2 (1.7)	9.8 (0.6)
M7_G_150	0.044	7	1.07	0.1540	150	20.7 (1.1)	1.9 (0.09)	16.2 (0.9)	2.3 (0.2)
M3_C_EA_20 <sup>1</sup>	0.095	3	3	0.1425	20	21.7 (0.5)	2.4 (0.05)	39.2 (1.7)	9.8 (0.6)
M3_C_EA_150	0.095	3	3	0.1425	150	20.7 (1.1)	1.9 (0.09)	16.2 (0.9)	2.3 (0.2)
<i>FRP-retrofitted</i>									
R1_C_20 <sup>1</sup>	0.095	1	1	0.0475	20	21.7 (0.3)	2.4 (0.05)	–	–
R1_C_150	0.095	1	1	0.0475	150	20.1 (0.7)	2.2 (0.1)	–	–
R3_C_20 <sup>1</sup>	0.095	3	3	0.1425	20	21.7 (0.3)	2.4 (0.05)	–	–
R3_C_150	0.095	3	3	0.1425	150	20.1 (0.7)	2.2 (0.1)	–	–
R7_BCo_20 <sup>1</sup>	0.0371	7	1.06	0.1299	20	21.7 (0.3)	2.4 (0.05)	–	–
R7_BCo_150	0.0371	7	1.06	0.1299	150	20.1 (0.7)	2.2 (0.1)	–	–
R7_G_20 <sup>1</sup>	0.044	7	1.07	0.1540	20	21.7 (0.3)	2.4 (0.05)	–	–
R7_G_150	0.044	7	1.07	0.1540	150	20.1 (0.7)	2.2 (0.1)	–	–
R3_C_EA_20 <sup>1</sup>	0.095	3	3	0.1425	20	21.7 (0.3)	2.4 (0.05)	–	–
R3_C_EA_150	0.095	3	3	0.1425	150	20.1 (0.7)	2.2 (0.1)	–	–

\* Textile thickness.

\*\* Axial stiffness of bare coated basalt or glass fibres textiles (axial stiffness of one layer times the number of layers) divided by the axial stiffness of one layer of dry carbon fibres textile.

\*\*\* Textile reinforcement ratio (as a percentage) which calculated as follows:  $\rho_f = A_f/bh$ , where  $b$  and  $h$  are the width and height of the beam respectively.  $A_f$  is the cross-sectional area of the textile fibres, the area of fibres is the product of  $t^*b$ , where  $t^*$  is the equivalent thickness of textile fibres and  $b$  is the beam width.

<sup>†</sup> Standard deviation in parenthesis.

<sup>1</sup> Specimens included in Raof et al. 2017 [11].

tensile strength were obtained (on the day of testing) by testing (three) cylinders with dimensions of 150 mm-diameter and 300 mm-height. The test was conducted according to the EN 12390-3 and EN 12390-6 [37,38] standards, respectively. The results are presented in Table 1. The yield stress, ultimate strength and rupture strain of the 8 mm-diameter (which was used as a longitudinal reinforcement and shear links reinforcement) was 568 MPa, 630 MPa and 7.9%, respectively. These values were experimentally measured and constitute the average values from three specimens. The corresponding values for the 12 mm-diameter bars (compression reinforcement) were 561 MPa, 637 MPa and 12.8%.

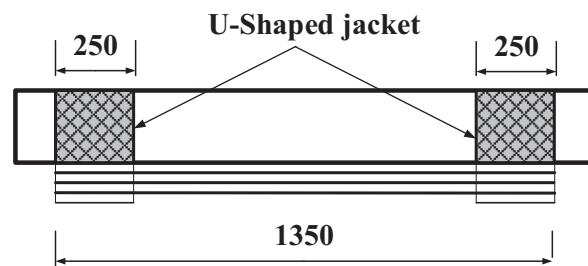
Three different textile materials were used as external reinforcement, namely carbon-fibre textile (dry and coated), basalt fibre-textile (coated) and glass-fibre textile (dry). All textiles

comprised fibre rovings fabricated in two orthogonal directions with the same amount of fibres in each direction. Details of the textiles, such as weight, mesh size and nominal thickness, are presented in Fig. 3a-c. It is noted that the values of nominal textile thicknesses in Fig. 3 were calculated based on the equivalent smeared distribution of fibres.

For TRM retrofitted specimens, the binding material comprising an inorganic binder consisting of cement and polymers at a ratio of 8:1 by weight. The water-cement ratio was 0.23 by weight, resulting in plastic consistency and good workability. The flexural and compressive strength of the mortar were experimentally obtained on the day of testing both at ambient and 150 °C. The tests were carried out on mortar prisms with dimensions of 40 × 40 × 160 mm according to EN 1015-11 [39] and are presented in Table 1. For the FRP-strengthened beams, a commercial

Textile material	TRM		FRP		Strengthening configuration
	Temperature		Temperature		
	20 °C	150 °C	20 °C	150 °C	
Carbon Fibres	M1_C_20 M1_CCo_20 M3_C_20	M1_C_150 M1_CCo_150 M3_C_150	R1_C_20 R3_C_20	R1_C_150 R3_C_150	
Coated basalt Fibres	M7_BCo_20	M7_BCo_150	R7_BCo_20	R7_BCo_150	
Glass Fibres	M7_G_20	M7_G_150	R7_G_20	R7_G_150	
Carbon Fibres+ End anchorage	M3_C_EA_20	M3_C_EA_150	R3_C_EA_20	R3_C_EA_150	

(a)



(b)

Fig. 2. (a) Group of specimens; (b) details of end anchorage system (dimensions in mm).

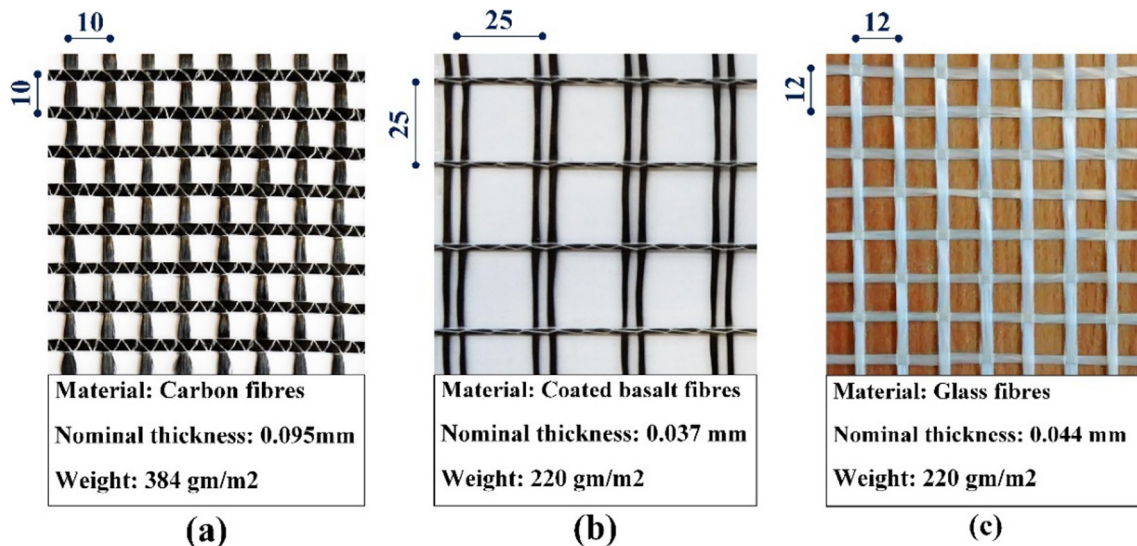
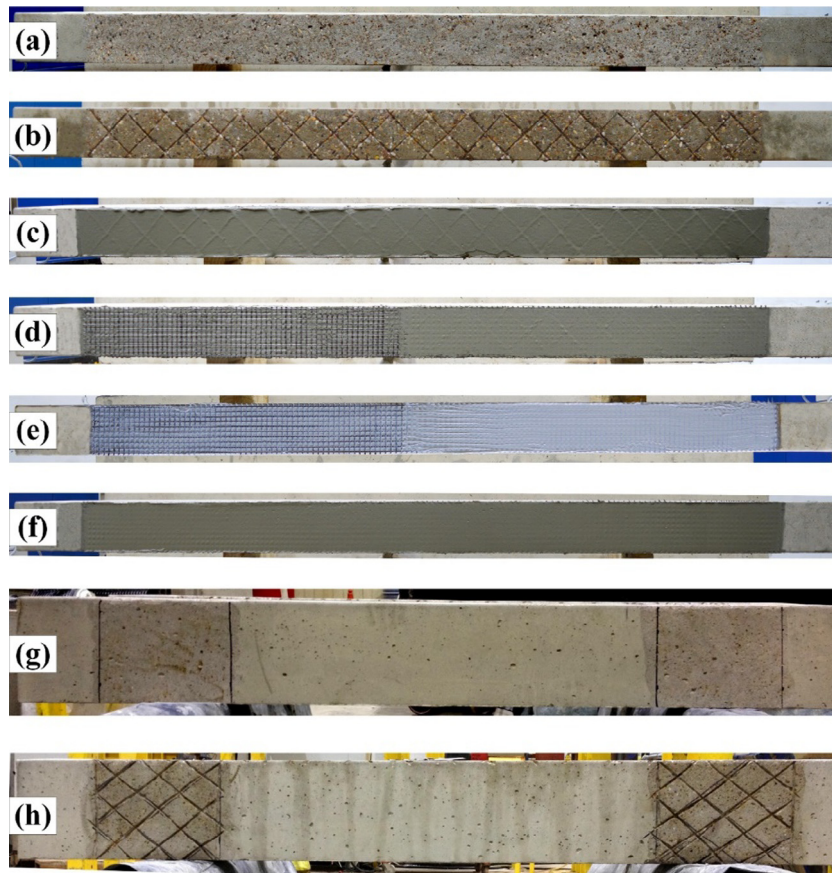


Fig. 3. Textiles used in this study: (a) carbon fibres textile; (b) glass fibres textile; (c) coated basalt fibres textile (dimensions in mm).

epoxy resin with tensile strength and modulus of elasticity of 30 MPa and 3.8 GPa, respectively, whereas its  $T_g$  is equal to 68 °C, (according to the manufacturer datasheets).

The strengthening material (TRM or FRP) was bonded to the beams' soffit over a length of 1350 mm (Fig. 1a). The strengthening procedure for both strengthening systems had the characteristics of a typical wet lay-up application as

described in Fig. 4a-h. For specimen M1\_CCo\_150, which was retrofitted with coated carbon-fibre textile, the dry carbon textile was impregnated with a low viscosity epoxy resin using a plastic roll two days prior to strengthening. The tensile strength and the elastic modulus of this adhesive were equal to 72.4 MPa and 3.18 GPa, respectively (according to the manufacturer data sheets).



**Fig. 4.** Strengthening procedure: (a) surface preparation of FRP-strengthened beams, (b) surface preparation of TRM-retrofitted beams, (c) application of first layer of mortar, (d) application of first layer of TRM, (e) application of the first layer of FRP, (f) application of final layer of mortar for TRM reinforced specimens, (g) surface preparation of FRP U-shaped jacket, (h) surface preparation for TRM U-shaped jacket.

### 2.3. Experimental setup

#### 2.3.1. Development of the heating system

Fig. 5a shows the heating system designed and manufactured to provide heating along the critical flexural span of the beams. The heating system comprised five 1000 W ceramic heaters of 60 mm width, 245 mm length and 30 mm thickness. The maximum surface temperature for each single heater is about 700 °C. The heaters were fixed to steel boxes which also facilitated the wiring of the heaters to the power supply (Fig. 5a). Those steel boxes were then mounted to a steel frame (Fig. 5b) with a length of 1350 mm, namely equal to length of the strengthened area of the beams. The steel frame was designed to be portable for allowing fast removal of the heating system from underneath the beams in case of emergency. At the same time the steel frame legs height was adjustable for controlling the distance between the heaters and beam's soffit. Moreover, to protect the heaters from falling parts of concrete and TRM or FRP in case of abrupt failures, a protection steel cage was fixed at the top the steel frame, as illustrated in Fig. 5a.

#### 2.3.2. Testing protocol and instrumentations

All beams were simply supported and subjected to four-point bending (Fig. 5c). As shown in Fig. 1a, the flexural span was 1500 mm, and the selected configuration resulted in a 340 mm-long constant moment zone and a 580 mm-long shear span. The load was applied using a 100 kN-capacity servo-hydraulic actuator which was fixed on a stiff reaction frame. A picture of the test setup is shown in Fig. 5c. The beams were subjected to a monotonic load-

ing under displacement control at a rate of 1 mm/min. Two LVDTs were fixed at the mid-span of the beam (one on each side) to measure independently the mid-span deflection.

For all FRP/TRM strengthened beams tested at high temperature, five type K thermocouples were mounted to the concrete surface prior to the application of the strengthening materials in order to monitor the temperature at concrete – adhesive interface. As shown in Fig. 5d, the thermocouples were distributed along the critical strengthened flexural span to ensure that the targeted temperature (i.e. 150 °C) is uniformly reached along that span. The test procedure at high temperature included the following steps: the heating system was placed underneath the specimen; the height of the legs was adjusted in order to achieve a distance of 100 mm (to allow for beam's deflection) between the heaters and the beam's soffit (Fig. 5c). The specimen was heated up to the pre-defined temperature (i.e. 150 °C), and then loaded monotonically up to failure, while the temperature at the concrete – adhesive interface was approximately kept constant at 150 °C. The data of the tests was recorded using a fully-computerized data acquisition system.

#### 2.3.3. Temperature profile

Fig. 6a and b shows typical time-temperature curves obtained from the five thermocouples (affixed at the concrete-adhesive interface) for specimens R3\_C\_150 and M3\_C\_150, respectively. It can be observed that: (a) the heating rate was approximately identical between the two specimens, (b) the temperature measured along the critical flexural span was consistent indicating the effectiveness of the heating system, and (c) the maximum variation of

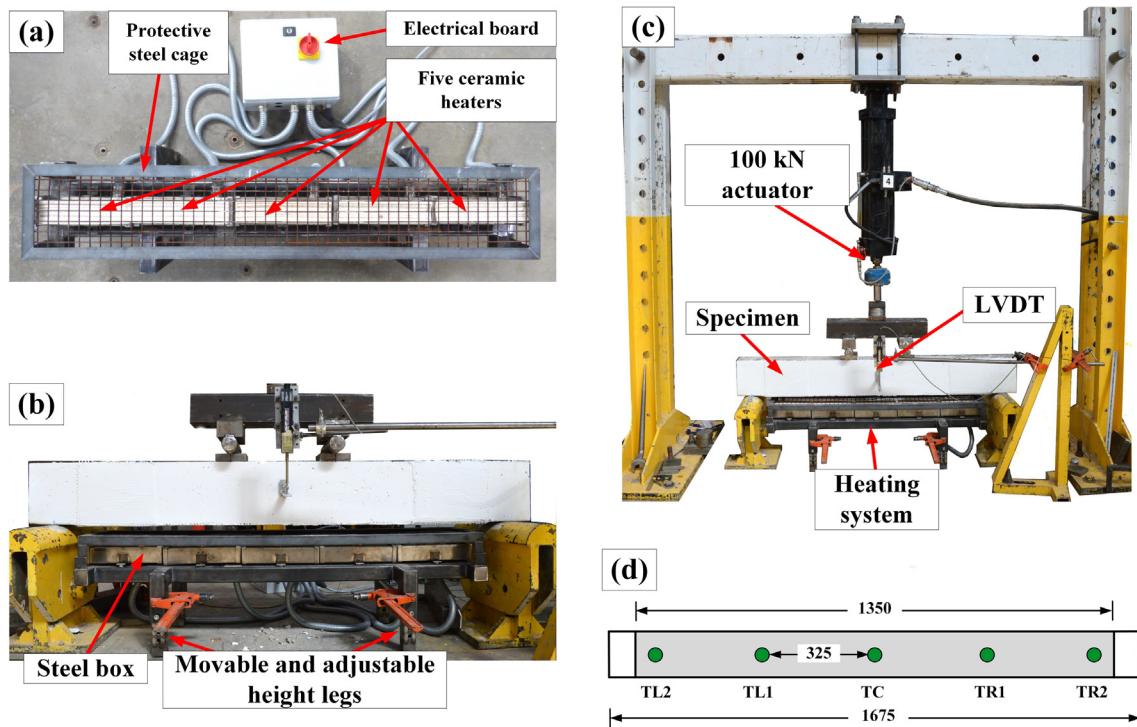


Fig. 5. Test setup: (a) heating system; (b) front view; (c) distribution of thermocouples along the strengthened area; (d) overall test setup.

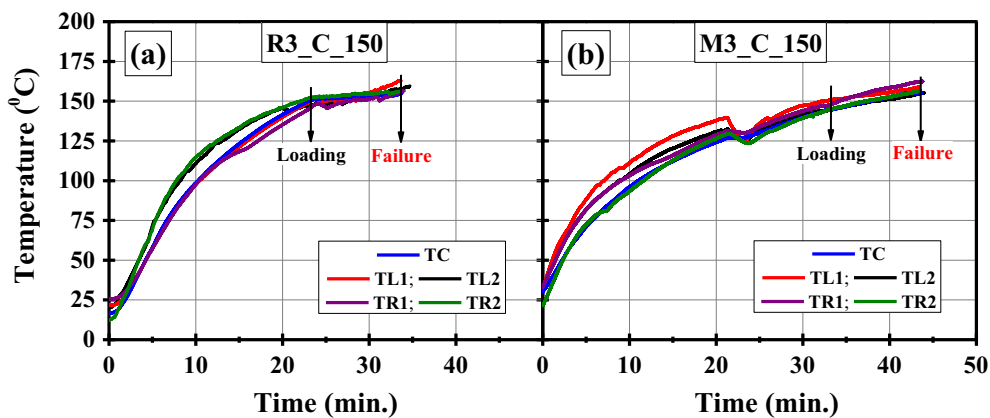


Fig. 6. Temperature-time curves: (a) FRP-strengthened beam (R3\_C\_150), and (b) TRM-retrofitted beam (M3\_C\_150).

temperature from the targeted one during all tests was approximately 7 °C (see Fig. 6a, b). Note that the consistency in the heating procedure for all tested specimens is important to reduce errors, obtain reliable and comparable results, and hence increase the level of confidence in the obtained results.

### 3. Experimental results

Table 2 summarizes the main results of all tested beams both at ambient temperature and 150 °C. The results of ambient temperature tests include: (1) The ultimate recorded load ( $P_u$ ). (2) The flexural capacity increases due to application of the strengthening. (3) The observed failure mode. Whereas, the results of the high temperature tests comprise: (1) The cracking load ( $P_{cr}$ ). (2) The yield load ( $P_y$ ) (which is defined as the load corresponding to the steel yielding). (3) The ultimate recorded load ( $P_u$ ). (4) The displacement corresponding to cracking load ( $\delta_{cr}$ ). (5) The

displacement corresponding to the yielding load ( $\delta_y$ ) (average mid-span deflection from two LVDTs corresponding to  $P_y$ ). (6) The displacement at ultimate load ( $\delta_u$ ) (average of mid-span deflection from two LVDTs at the ultimate load ( $P_u$ )). (7) The flexural capacity increase due to strengthening. (8) The observed failure mode. The last column in Table 2 reports the reduction of the contribution of FRP/TRM reinforcement (as a percentage) to the total flexural capacity due to the effect of high temperature, expressed by the ratio,  $(f_{c, AT} - f_{c, HT})/f_{c, AT}$ .

#### 3.1. Load-displacement curves

The response of all beams tested at ambient and high temperature is presented in Fig. 7a-c in the form of load-displacement curves, which are characterized by three distinct stages: (1) Stage I: un-cracked beam; (2) Stage II: initiation of cracking up to steel yielding; and (3) Stage III: post-yielding response up to failure.

**Table 2**  
Summary of test results of beams tested at ambient temperature and at 150 °C.

Specimen	Ambient temperature (20 °C)			Ambient temperature (150 °C)						(7) Flexural capacity increase $f_{c, HT}$ (%)	(8) Failure mode <sup>a</sup>	$(f_{c, AT} - f_{c, HT}) / f_{c, AT}$ (%)	
	(1) Ultimate load ( $P_u$ )	(2) Flexural capacity increase ( $f_{c, AT}$ ) (%)	(3) Failure mode <sup>a</sup>	Load (kN)			Deflection (mm)						
				(1) Crack ( $P_{cr}$ )	(2) Yield ( $P_y$ )	(3) Ultimate ( $P_u$ )	(4) Crack ( $\delta_{cr}$ )	(5) Yield ( $\delta_y$ )	(6) Ultimate ( $\delta_u$ )				
CON	34.6	–	CC	–	–	–	–	–	–	–	–	–	–
<i>TRM-retrofitted</i>													
M1_C	39.0	12.7	S	6.8	35.2	37.7	0.7	7.1	9.1	9.0	S	29.5	
M1_CCo	41.3	19.4	ID	8.0	34.4	38.3	0.6	5.9	8.1	10.7	ID	44.8	
M3_C	55.3	59.8	D	7.4	34.7	44.7	0.74	6.1	8.9	29.2	D	51.2	
M7_BCo	46.9	35.5	FR	10.8	34.5	41.1	1.15	6.1	13.7	18.8	S	47.2	
M7_G	43.2	24.9	FR	7.6	36.8	38.8	0.67	7.2	10.3	12.1	S	51.2	
M3_C_EA	57.1	65.0	DS	11.3	41.4	46.2	0.93	7.43	10.5	33.5	DS	48.4	
<i>FRP-retrofitted</i>													
R1_C	43.9	26.9	D	8.8	34.4	35.9	0.74	6.5	8.7	3.8	AF	86.0	
R3_C	60.4	74.6	D	8.2	35.6	36.7	0.61	6.7	8.2	5.8	AF	92.2	
R7_BCo	54.2	56.6	FR	8.0	33.6	36.5	0.8	6.3	11.6	5.5	AF	90.3	
R7_G	48.2	39.3	FR	7.5	29.8	35.8	0.4	5.6	19.45	3.5	AF	91.2	
R3_C_EA	83.7	141.9	FR	10.0	42.6	57.5	0.53	6.8	25	66.2	AS	53.4	

<sup>a</sup> CC: Concrete crushing; S: slippage and partial rupture of the fibres through the mortar; ID: TRM debonding at the textile/mortar interface (inter-laminar shearing); D: TRM debonding from concrete substrate including parts of concrete cover; AF: adhesive failure at the concrete–resin interface; DS: Debonding of TRM from concrete substrate, followed by slippage of the fibres at the region where the longitudinal TRM meets the TRM U-jacket; and AS: adhesive failure at the concrete–resin interface in the non-anchorage zone followed by partial rupture and slippage of the fibres at the region where the longitudinal FRP meets the FRP U-jacket.

The observed gain in flexural strength is due to the contribution of TRM/FRP reinforcement, and is completely lost after the peak-load (when this reinforcement is lost), with the load capacity dropped to the un-retrofitted (CON) beam level.

### 3.2. Ultimate load and failure mode

The control specimen (CON) sustained a peak load of 34.6 kN (Table 2) and failed in flexure. After yielding of the longitudinal reinforcement, the concrete in the compression zone crushed (Fig. 8a).

#### 3.2.1. FRP strengthened beams

All FRP-strengthened beams tested at ambient temperature failed in flexure at an ultimate load substantially higher than that of the control beam. The peak load recorded for specimens R1\_C\_20, R3\_C\_20, R7\_BCo\_20, R7\_G\_20, and R3\_C\_EA\_20 was 43.9, 60.4, 54.2, 48.2, and 83.7 kN, respectively, yielding 26.9, 74.6, 56.6, 39.3, and 141.9% gain in load-carrying capacity, respectively (Table 2). Two different failure modes were observed, namely: debonding of FRP from the beam's soffit including part of the concrete cover (Fig. 8b–specimens R1\_C\_20 and R3\_C\_20), and rupture of the fibres at the constant moment region of the beam (Fig. 8d, f and h – specimens R7\_BCo\_20, R7\_G\_20, and R3\_C\_EA\_20, respectively).

All FRP-retrofitted beams tested at 150 °C failed also in flexure but at ultimate loads significantly lower (except from specimen R3\_C\_EA\_150) than their counterpart specimens tested at 20 °C. The peak load attained by specimens R1\_C\_150, R3\_C\_150, R7\_BCo\_150, and R7\_G\_150 was 35.9, 36.7, 36.5, and 35.8 kN (Table 2), respectively, resulting in negligible increases in the flexural capacity equal to 3.8, 5.8, 5.5, and 3.5%, respectively. Thus, the effectiveness of FRP reinforcement in increasing the flexural capacity of the beams was decreased (in average) by 90% at 150 °C in comparison with ambient temperature. In all of these specimens, adhesive failure at the concrete–resin interface was observed (Fig. 8c, e and g), namely the FRP composite detached from concrete substrate without including any parts of concrete cover. This is attributed to the poor bond behaviour of epoxy resin at temper-

atures above  $T_g$ . Finally, specimen R3\_C\_EA\_150 having an anchorage system provided by U-shaped FRP strip at the ends of the beam attained an ultimate load of 57.5 kN, which yields 53.4% reduction in the effectiveness of the FRP reinforcement compared to its corresponding ambient temperature. Failure of this specimen initiated by adhesive failure at the concrete – resin interface in the mid-span which propagated to the anchorage zones, and then followed by slippage and partial rupture of the rovings through the resin, which lost its strength at high temperature (Fig. 8i).

#### 3.2.2. TRM strengthened beams

Similar to the FRP strengthened beams, the TRM ones tested at ambient temperature, sustained considerably higher loads than the control beam. The ultimate load – carrying capacity of specimens M1\_C\_20, M1\_CCo\_20, M3\_C\_20, M7\_BCo\_20, M7\_G\_20 and M3\_C\_EA\_20 was 39, 41.3, 55.3, 46.9, 43.2, and 57.1 kN, respectively, resulting an increase in the flexural capacity of 12.7, 19.4, 59.8, 35.5, 24.9, and 65.0% in comparison with the control beam. Five different failure modes were observed depending on the investigated parameters. In particular, failure of specimen M1\_C\_20 was attributed to partial rupture and slippage of the fibres within the mortar (Fig. 9a), whereas in specimen M1\_CCo\_20, the failure occurred at the textile–mortar interface due to shearing of the mortar (interlaminar shearing, Fig. 9c). Failure of specimen M3\_C\_20 was identical to R3\_C\_20, namely due to TRM debonding including part of the concrete cover (Fig. 9e). Failure due to rupture of textile glass and basalt fibres was respectively observed in both M7\_BCo\_20 and M7\_G\_20 specimens (Fig. 9g and i). Finally, specimen M3\_C\_EA\_20 failed due to TRM debonding from concrete substrate, followed by slippage of the fibres at the region where the longitudinal TRM meets the TRM U-jacket (Fig. 9k).

The performance of the TRM-strengthened beams tested at 150 °C was far better compared to their FRP counterparts. In particular, specimens M1\_C\_150, M1\_CCo\_150, M3\_C\_150, M7\_BCo\_150, M7\_G\_150 and M3\_C\_EA\_150, reached an ultimate load of 37.7, 38.3, 44.7, 41.1, 38.8, and 46.2 kN, respectively, resulting in 9, 10.7, 29.2, 18.8, 12.1, and 33.5% increase in the flexural capacity. Consequently, the effectiveness of the TRM at 150 °C

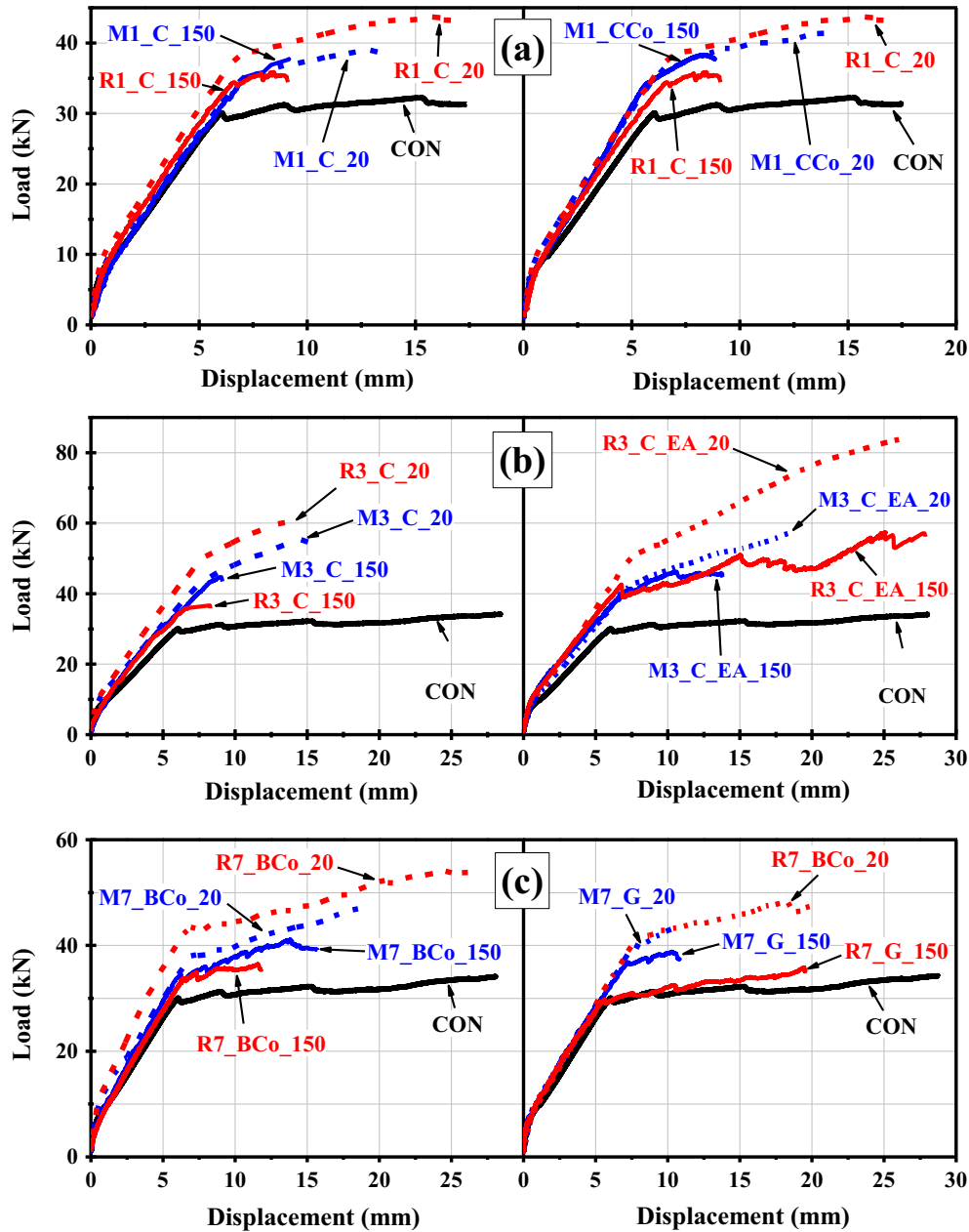


Fig. 7. Load versus mid-span deflection curves of beams tested at ambient and high temperature and strengthened with: (a) one layer of carbon fibres textile, (b) three layers of carbon fibres textile without and with providing end-anchorage system, and (c) seven layers of basalt or glass fibres textile.

was decreased in average by about 45% in comparison with its performance at 20 °C.

Specimen M1\_C\_150, failed identically to its counterpart tested at 20 °C due to partial rupture and slippage of the fibre rovings through the mortar (Fig. 9b). Specimen M1\_CCo\_150 failed due to debonding of TRM at the textile-mortar interface (Fig. 9d) similar to its counterpart specimen tested at ambient temperature. Specimen M3\_C\_150 failed also identically to its counterpart M3\_C\_20, namely TRM debonding from the concrete substrate involving parts of concrete cover (Fig. 9f), indicating the good bond between the concrete substrate and the TRM reinforcement even at high temperature. Specimens M7\_BCo\_150 and M7\_G\_150 had different failure modes compared to their counterpart specimens tested at 20 °C, as they failed due to slippage of textile fibres (although some debonding was observed in specimen M7\_G\_150) through the mortar (Fig. 9h and j). The alteration of

failure mode is attributed to the reduction of the mortar strength at high temperature (see Table 1). Finally, the failure mode of specimen M3\_C\_EA\_150 was also identical to its counterpart M3\_C\_EA\_20 that is debonding of TRM from concrete substrate, followed by slippage of the fibres at the region where the longitudinal TRM meets the TRM U-jacket (Fig. 9l).

#### 4. Discussion

All specimens behaved as designed and failed in flexural, by failure of the EB TRM/FRP reinforcement after yielding of the internal steel reinforcement. In terms of the various parameters investigated in this experimental programme, an examination of the results in terms of flexural capacity, and failure modes, revealed the following information.

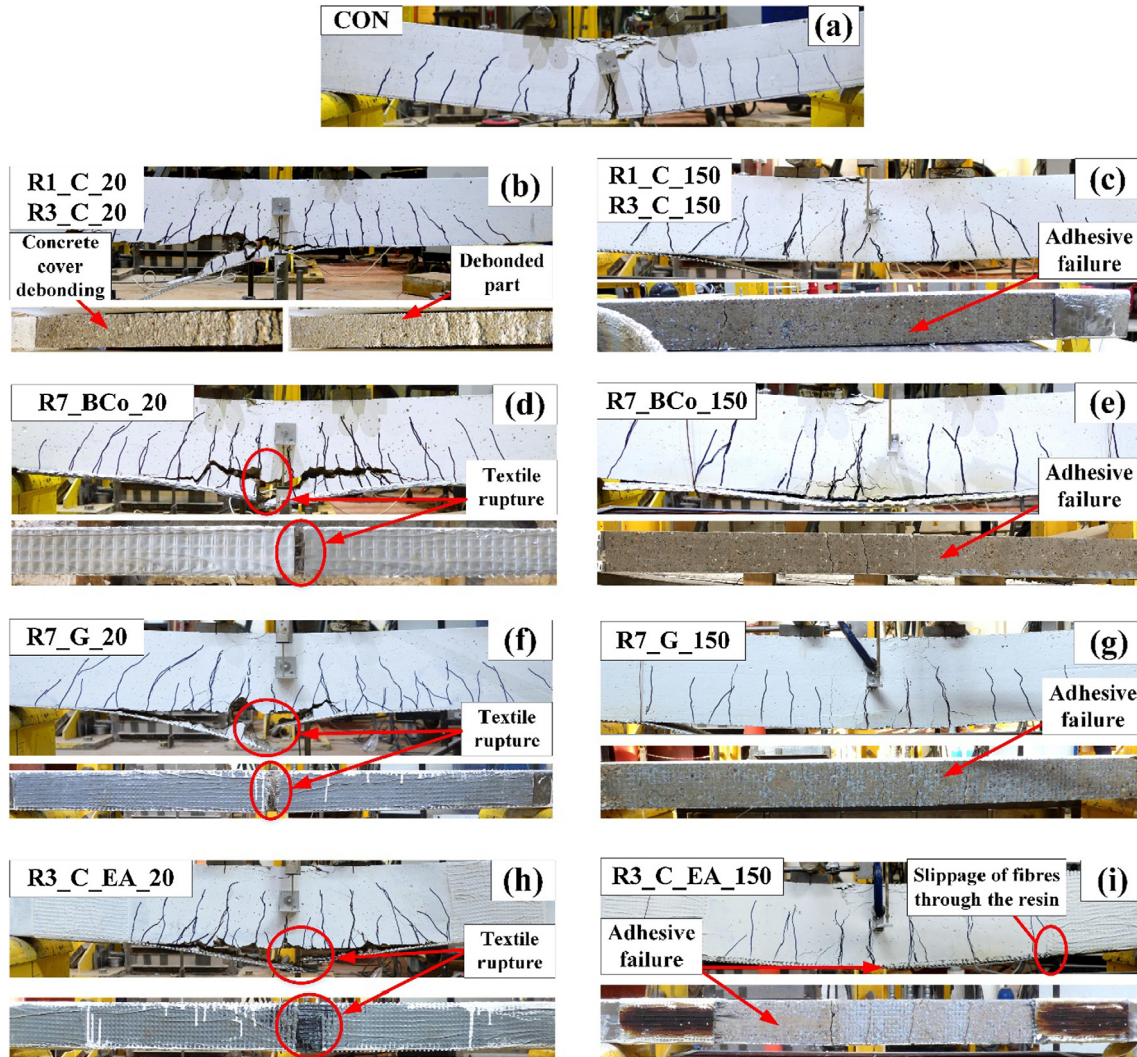


**Fig. 8.** Failure modes observed in: (a) Un-retrofitted beam; and FRP strengthened beams with: (b and c) 1 and 3 layers of carbon; (d and e) 7 layers coated basalt, (f and g) 7 layers glass, and (h and i) 3 layers carbon provided with end-anchorage; tested at 20 °C and 150 °C, respectively.

#### 4.1. Matrix material (TRM vs. FRP): performance at high temperature

FRP was more effective than TRM in increasing the flexural capacity of RC beams at ambient temperatures, however at high temperature TRM outperformed FRP (Fig. 10a-c), maintaining on average of 55% of its effectiveness at ambient temperature, whereas, FRP maintained only 10% (Fig. 11). This reduction in effectiveness is clearly related to bigger deterioration in the epoxy resin mechanical properties at high temperatures in comparison with the mortar.

In the next sections a comparison between the effectiveness of FRP vs. TRM materials at high temperatures in terms of the number of layers, the textile fibres materials, and the end-anchorage system is made. The effect of textile coating on the performance of TRM strengthened specimens in increasing the flexural capacity will also be discussed.

#### 4.2. Number of strengthening layers

The effect of the number of TRM layers on the beams flexural capacity enhancement at high temperature was investigated only for the case of dry carbon-fibre textiles, and is depicted in Fig. 12. Increasing the number of layers from 1 to 3 layers, resulted in an almost proportional enhancement in the flexural capacity of

3.25 times. For FRP specimens the corresponding increase was nearly zero as can be seen in Figs. 12 and 10a. When the number of TRM layers was increased from one to three, the failure mode altered from local fibre slippage to TRM debonding with concrete cover due to the better mechanical interlock [15], for both ambient and high temperatures, indicating that the failure mode was not affected from the increase of the temperature. For FRP strengthened specimens however, the increase in the number of layers did not affect the failure mode, which was adhesive at the concrete-resin interface (Fig. 8c), attributed to the deterioration of the epoxy tensile strength above the  $T_g$ , as also reported in bond tests [34].

#### 4.3. Textile fibre coating

Coating was applied to the dry carbon-fibres textile to prevent the premature failure due to slippage of the fibre that was observed with dry carbon fibres textile. As a result of coating, the flexural capacity of specimen M1\_CCo\_150 was further increased by 19% compared to specimen M1\_C\_150. In fact, the effectiveness of the coated carbon textile was dropped compared to its effectiveness at ambient temperature (52%), most possibly due to the adverse effect of high temperature on the properties of the epoxy resin that used for coating.

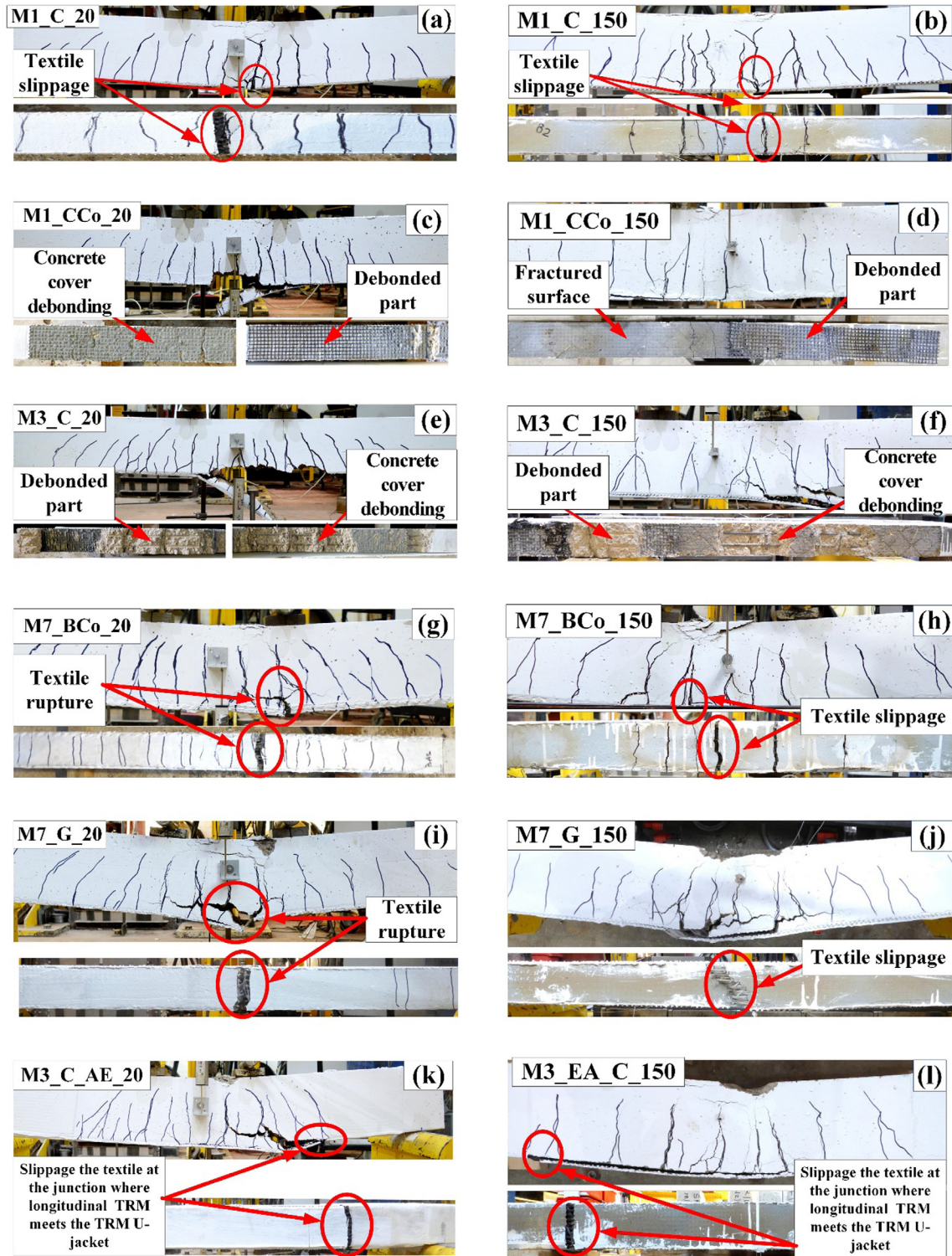


**Fig. 9.** Failure modes of TRM strengthened beams with: (a and b) 1 layer dry carbon, (c and d) 1 layer coated carbon, (e and f) 3 layers of carbon, (g and h) 7 layers coated basalt, (i and j) 7 layers of glass, and (k and l) 3 layers carbon provided with end-anchorage; tested at 20 °C and 150 °C, respectively.

The failure mode was altered from slippage to TRM debonding at the textile-mortar interface (Fig. 9d) because coating the textile improved the bond between the inner and outer filaments, and hence, prevented slippage. Identical failure mode was also observed at ambient temperature [11], indicating that the failure mode was not affected from the increase of the temperature.

#### 4.4. Textile fibre material

No clear conclusions on the influence of the textile fibre material can be made at high temperatures. The behaviour of the FRP strengthened beams was controlled by the adhesive failure at the concrete-resin interface (see Section 4.1). Whereas the flexural capacity increases for TRM strengthened specimens that received

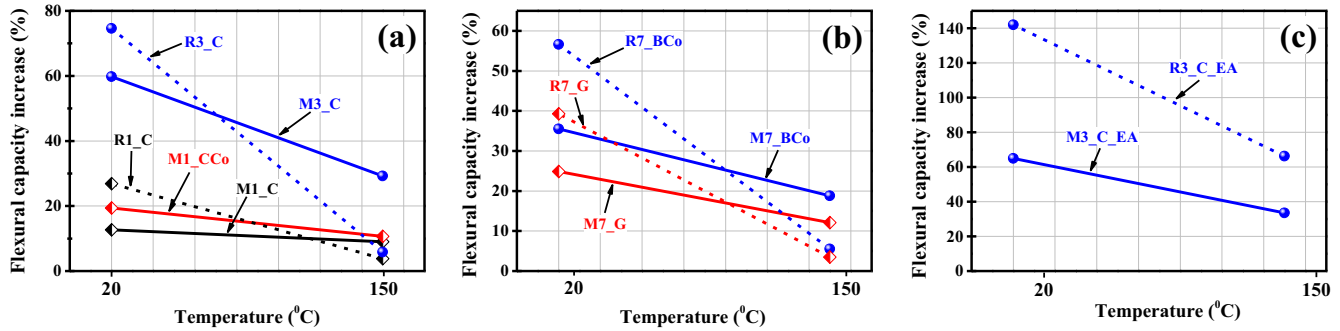


Fig. 10. Effect of temperature on the flexural capacity enhancement for both TRM and FRP system.

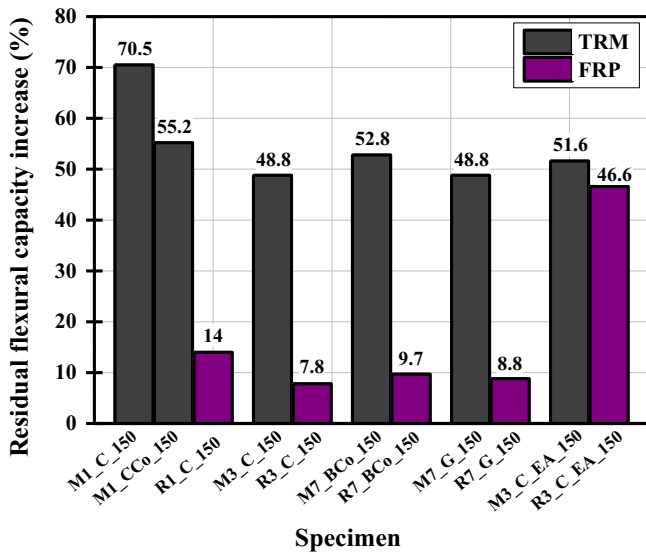


Fig. 11. Comparison of residual flexural capacity increase of TRM vs. FRP strengthened beams at 150 °C.

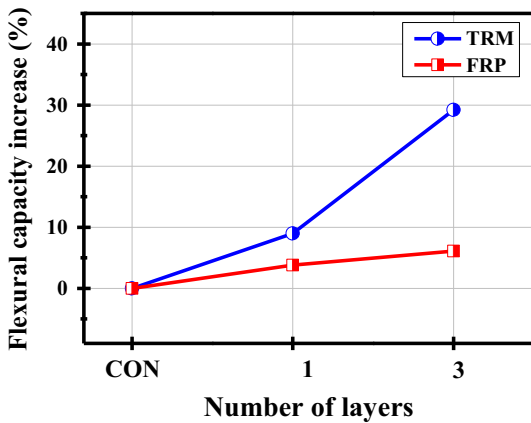


Fig. 12. Effect of the number of layers on the ultimate flexural capacity at 150 °C.

reinforcement with the same axial stiffness (M7\_BCo vs. M1\_CCo\_150 and M7\_G\_150 vs. M1\_C\_150), are mainly attributed to the effect of the increased number of layers (see Section 4.2), rather the material properties themselves.

4.5. End-anchorage with U-jackets

Providing end-anchorage enhanced significantly the effectiveness of FRP at high temperature (11.4 times compared to the

non-anchorage beam). This improvement is mainly related to the effect of the cold anchorage zones as also observed in [36]. The corresponding enhancement for the TRM-strengthened beams was ten times less (only 1.14) due to slippage of the textile fibres at the junction where the longitudinal TRM meets the U-jacket.

4.6. TRM vs. FRP effectiveness factor

Table 3 reports the values of TRM vs. FRP effectiveness factor ( $\alpha_{HT}$ ) at high temperature, which is defined as the ratio of the TRM to FRP in terms of flexural capacity enhancement. This factor was varying between 0.5 and 5.1 depending on the investigated parameter. Increasing the number of layers from one to three (for dry carbon fibres textile), resulted in an increase of the  $\alpha_{HT}$  factor from 2.4 to 5.1 (2.12 times) due to the change in failure mode, as discussed in Section 4.2. On the other hand, coating the dry carbon textile in the case of one TRM layer increased the  $\alpha_{HT}$  factor from 2.4 to 2.8 due to prevention of slippage of the fibres. The effectiveness factor  $\alpha_{HT}$  for both specimens that received 7 basalt or glass TRM (M7\_BCo\_150 and M7\_G\_150) was approximately the same (about 3.4) due to their identical failure mode (slippage of fibres through the mortar). Finally, the low value of 0.5 for specimen M3\_C\_EA\_150 that received end-anchorage, is related to the observed failure mode (see Section 3.2.2).

5. Effective stress reduction factor for FRP and TRM

The effective stress is defined here as the tensile stress of the composite material in the region of maximum moment at the instant of ultimate load. For all beams tested, the effective stress of the FRP or TRM reinforcement was calculated using an inverse analysis method for both ambient ( $\sigma_{eff}$ ) and high ( $\sigma_{eff, high}$ ) temperatures. By using the experimental values of the flexural moment of resistance,  $M_{u,exp}$  (Table 3), a standard cross section analysis, described in fib Model Code 2010 [40], was performed for each of the retrofitted beams. The procedure for the calculation of  $\sigma_{eff}$  and  $\sigma_{eff, high}$  in this method is based on the equilibrium of internal forces, strains compatibility, and on the assumptions of: perfect bond between the strengthening layers and the concrete substrate; ultimate compressive strain of concrete ( $\epsilon_{cu}$ ) equal to 0.0035; and linear elastic behaviour of the strengthening material up to failure. The mechanical properties of the FRP/TRM reinforcement ( $E_f$  and  $f_{fu}$ ) were taken from the coupon tests reported in Raof et al. 2017 [11] and are presented in Table 3.

The effective stress of FRP or TRM jackets at high temperature,  $\sigma_{eff, high}$ , is a reduced value of their effective stress,  $\sigma_{eff}$ , at ambient temperature. It is expressed by the following equation:

$$\sigma_{eff, high} = k\sigma_{eff} \tag{1}$$

**Table 3**  
Effectiveness factor, experimental values of ultimate moment capacity and effective stress in TRM/FRP reinforcement.

Specimen	TRM vs. FRP effectiveness factor, $\alpha_{HT}$	$f_{fu}^+$ (MPa)	$M_{u,exp.}$ kN.m	A.T. $\sigma_{eff}^{**}$	H.T. $\sigma_{eff,high}^{***}$	$k^a$
CON	–		10.03	–		
<i>TRM-retrofitted</i>						
M1_C_150	2.4	1518	10.93	1368	1301	0.95
M1_CCo_150	2.8	2843	11.11	1825	1404	0.77
M3_C_150	5.1	1518	12.96	1434	834	0.58
M7_BCo_150	3.4	1190	11.92	1019	637	0.63
M7_G_150	3.5	794	11.25	658	411	0.62
M3_C_EA_150	0.5	1518	13.40	1501	934	0.62
<i>FRP-retrofitted</i>						
R1_C_150	n.a.	2936	10.41	2190	576	0.26
R3_C_150	n.a.	2936	10.61	1796	338	0.19
R7_BCo_150	n.a.	1501	10.59	1493	298	0.20
R7_G_150	n.a.	1019	10.38	914	257	0.28
R3_C_EA_150	n.a.	2936	16.68	3110	1577	0.51

<sup>+</sup> Ultimate tensile stress of the FRP/TRM reinforcement (MPa) obtained from coupon tests included in [11].

<sup>\*</sup> Ultimate moment capacity obtained experimentally.

<sup>\*\*</sup> Effective stress in TRM/FRP reinforcement calculated based on experimental results (at ambient temperature) included in [11].

<sup>\*\*\*</sup> Effective stress in TRM/FRP reinforcement calculated based on experimental results (at high temperature).

<sup>a</sup> The ratio of effective stress at high temperature ( $\sigma_{eff, high}$ ) to the effective stress at ambient temperature ( $\sigma_{eff}$ ).

The values of the effective stress of TRM and FRP jackets at both ambient and high temperature,  $\sigma_{eff}$  and  $\sigma_{eff, high}$ , respectively are given in Table 3. The calculated stress reduction factor,  $k$  varies with the strengthening material (TRM, FRP) and investigated parameter (see Table 3). For the FRP strengthened beams, the average values of  $k$  was quite low and equal to 0.29, whereas, the corresponding values of  $k$  for TRM strengthened beams was far higher and equal to 0.7.

As reported in Raouf at al. 2017 [11], Eq. (2) which suggested by *fib Model Code 2010* [41] can satisfactory predicted the stress of the TRM composite, ( $f_{fbm,theor}$ ), (without safety factors) for those specimens failed due to debonding.

$$f_{fbm} = k_c k_m k_b \beta_\ell \sqrt{\frac{2E_f}{t_f} f_{cm}^{2/3}} \quad (2)$$

In the above equation,  $f_{fbm}$  is the mean debonding stress of the composite material;  $k_c$  is the intermediate flexural crack factor and equal to 2;  $k_m$  is the matrix factor and equal to 0.25 for the case of epoxy bonded CFRP system (the same value was used here for the case of the carbon-TRM system);  $k_b$  is the shape factor and

is equal to 1;  $\beta_\ell$  is the length factor which can be taken equal to 1;  $E_f$  is the modulus of elasticity of the composite material (obtained from coupon test) presented in [11];  $t_f$  is the nominal thickness of the textile (see Table 1) and  $f_{cm}$  is the concrete compressive strength.

Fig. 13 shows the relationship between the effective stress at high temperature  $\sigma_{eff, high}$  and the product  $\rho_f E_f$ ; together with the curve corresponding to Eq. (2). Where  $\rho_f$  is the textile fibres reinforcement ratio ( $\rho_f = A_f/bh$ ), and  $E_f$  is the modulus of elasticity of the composite material obtained from coupon tests. It is clear from this Figure that Eq. (2) significantly overestimated the effective stress in FRP reinforcement due to the premature adhesive failure. Nevertheless, this was not the case in the TRM reinforcement where it seems that Eq. (2) can be used by providing a suitable reduction factor.

Hence, for design purposes, FRP is not recommended for flexural strengthening of RC beams when fire or high temperature is a critical issue, unless proper protective (thermal insulation) systems are provided. For TRM strengthened beams on the other hand, and based on the limited experimental results presented in this study in the flexural design of beams strengthened with

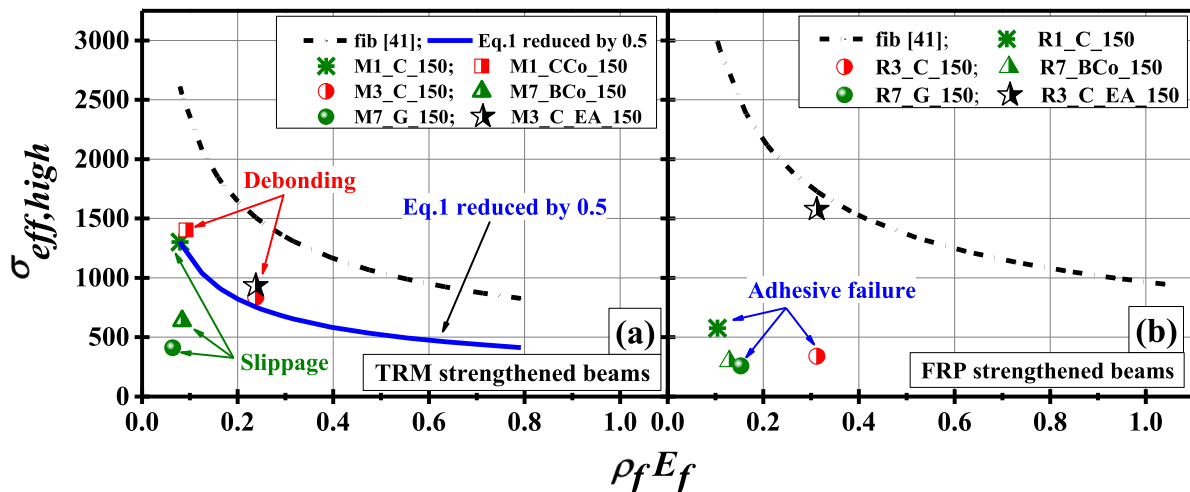


**Fig. 13.** Experimentally obtained effective stress versus  $\rho_f E_f$  and comparison with the theoretical formula suggested by *fib 2010* [41] and its modification for 150 °C for (a) TRM and (b) FRP strengthened beams.

TRM and exposed to high temperature (up to e 150 °C), the effective stress for those specimens failed due to debonding can be the minimum value obtained from coupon tests ( $f_{fu}$ ) and Eq. (2), after applying a reduction factor  $k$  equal to 0.5. It worth mentioning that a reduction factor of 0.4 was proposed by Tetta and Bournas 2016 [35] for shear design of beams strengthened with TRM jacketing and exposed to high temperature up to 250 °C. Finally, it is clear that more experimental data is required to suggest a design model taking into consideration different exposure temperatures and also different failure modes that observed in TRM strengthened beams tested at high temperature.

## 6. Conclusions

This study compares for the first time the effectiveness of TRM vs. FRP in increasing the flexural capacity of RC beams subjected to high temperature without protecting their anchorage zones. Parameters examined were: the strengthening system (TRM vs. FRP), the number of layers, the textile surface condition, the textile fibres materials and (e) the end anchorage system. The results of high temperature tests revealed the following information:

1. TRM showed far better effectiveness than FRP in increasing the flexural capacity of RC beams subjected to high temperature. TRM sustained an average of 55% of its ambient temperature effectiveness, contrary to FRP which totally lost its effectiveness.
2. Increasing the number of TRM layers (from 1 to 3) enhanced the flexural capacity and altered the failure mode. Whereas, the corresponding effect of the number of FRP layers was negligible due to the premature adhesive failure.
3. Coating the dry carbon fibres with epoxy adhesive improved the TRM effectiveness in increasing the flexural capacity (approximately 20% compared to the dry one).
4. The effect of textile materials (having approximate same axial stiffness) in the FRP-strengthened beams disappeared due to their identical adhesive failure at the resin-reinforcement interface.
5. Providing end-anchorage to the FRP-retrofitted beam significantly enhanced the flexural capacity increase (compared to the non-anchorage beam). This enhancement was limited in the corresponding TRM-reinforced beam due to the witnessed failure mode.
6. Different types of failure modes were observed in the TRM-retrofitted beams including: slippage of the fibres, interlaminar shear and debonding of TRM including parts of concrete cover. On the other hand, the only observed failure mode in the FRP strengthened specimens (except from specimen R3\_C\_EA\_150) was adhesive failure.
7. The *fib* 2010 formula [41], which predicted the experimental TRM debonding effective stress with good accuracy, can be also used in the flexural design of beams strengthened with TRM and exposed to high temperature (up to e 150 °C), after halving the ambient temperature effective stress.

The above conclusions were built based on limited number of half-scale beams and specific level of temperature. More studies are required by considering wide range of temperatures or simulating a real fire scenario. Testing full-scale beams are also needed in order to increase the level of confidence of the obtained results.

## Acknowledgements

The authors wish to thank the technical staff in the concrete lab, at the University of Nottingham for their assistance in the experi-

mental work. The authors would also like to present their gratitude to the post-doctoral research associate Lampros Koutas and Dr. Zoi Tetta. This work was supported by the Engineering and Physical Sciences Research Council (EPSRC) [grant number EP/L50502X/1] UK, and the research described in this research has been co-financed by the Higher Committee for Education Development in Iraq (HCED).

## References

- [1] V.K. Kodur, L.A. Bisby, M.F. Green, Experimental evaluation of the fire behaviour of insulated fibre-reinforced-polymer-strengthened reinforced concrete columns, *Fire Saf. J.* 41 (7) (2006) 547–557.
- [2] J.P. Firmo, J.R. Correia, L.A. Bisby, Fire behaviour of FRP-strengthened reinforced concrete structural elements: a state-of-the-art review, *Compos. B Eng.* 80 (2015) 198–216.
- [3] D.A. Bournas, P.V. Lontou, C.G. Papanicolaou, T.C. Triantafillou, Textile-reinforced mortar versus fiber-reinforced polymer confinement in reinforced concrete columns, *ACI Struct. J.* 104 (6) (2007) 740.
- [4] W. Bramehuber, State-of-the-art Report of RILEM Technical Committee 201 TRC: Textile Reinforced Concrete (RILEM Report 36), RILEM Publications SARL, Bagnaux, 2006.
- [5] C. Carloni, D.A. Bournas, F.G. Carozzi, T. D'Antino, G. Fava, F. Focacci, et al., Fiber reinforced composites with cementitious (inorganic) matrix. Design Procedures for the Use of Composites in Strengthening of Reinforced Concrete Structures, Springer, 2016, pp. 349–392.
- [6] A. D'Ambrisi, L. Feo, F. Focacci, Experimental analysis on bond between PBO-FRCM strengthening materials and concrete, *Compos. B Eng.* 44 (1) (2013) 524–532.
- [7] S.M. Raouf, L.N. Koutas, D.A. Bournas, Bond between textile-reinforced mortar (TRM) and concrete slabs: experimental investigation, *Compos. B Eng.* 98 (2016) 350–361.
- [8] A. D'Ambrisi, F. Focacci, Flexural strengthening of RC beams with cement-based composites, *J. Compos. Constr.* 15 (5) (2011) 707–720.
- [9] L. Ombres, Flexural analysis of reinforced concrete beams strengthened with a cement based high strength composite material, *Compos. Struct.* 94 (1) (2011) 143–155.
- [10] U. Ebead, K.C. Shrestha, M.S. Afzal, A. El Refai, A. Nanni, Effectiveness of fabric-reinforced cementitious matrix in strengthening reinforced concrete beams, *J. Compos. Constr.* 04016084 (2016).
- [11] S.M. Raouf, L.N. Koutas, D.A. Bournas, Textile-Reinforced Mortar (TRM) versus Fibre-Reinforced Polymers (FRP) in flexural strengthening of RC beams, *Constr. Build. Mater.* (2017), <http://dx.doi.org/10.1016/j.conbuildmat.2017.05.023>.
- [12] F. Schladitz, M. Frenzel, D. Ehlig, M. Curbach, Bending load capacity of reinforced concrete slabs strengthened with textile reinforced concrete, *Eng. Struct.* 40 (2012) 317–326.
- [13] G. Loreto, L. Leardini, D. Arboleda, A. Nanni, Performance of RC slab-type elements strengthened with fabric-reinforced cementitious-matrix composites, *J. Compos. Constr.* 18 (3) (2013) A4013003.
- [14] L.N. Koutas, D.A. Bournas, Flexural strengthening of two-way RC slabs with textile-reinforced mortar: experimental investigation and design equations, *J. Compos. Constr.* 04016065 (2016).
- [15] C. Papanicolaou, T.C. Triantafillou, I. Papantoniou, C. Balioukos, Strengthening of two-way reinforced concrete slabs with textile reinforced mortars (TRM), in: 4th Colloquium on Textile Reinforced Structures (CTRS4), Dresde, June 3–5, 2009.
- [16] Z.C. Tetta, L.N. Koutas, D.A. Bournas, Textile-reinforced mortar (TRM) versus fiber-reinforced polymers (FRP) in shear strengthening of concrete beams, *Compos. B Eng.* 77 (2015) 338–348.
- [17] T. Trapko, D. Urbańska, M. Kamiński, Shear strengthening of reinforced concrete beams with PBO-FRCM composites, *Compos. B Eng.* 80 (2015) 63–72.
- [18] Z.C. Tetta, L.N. Koutas, D.A. Bournas, Shear strengthening of full-scale RC T-beams using textile-reinforced mortar and textile-based anchors, *Compos. B Eng.* 95 (2016) 225–239.
- [19] O. Awani, T. El-Maaddawy, A. El Refai, Numerical simulation and experimental testing of concrete beams strengthened in shear with fabric-reinforced cementitious matrix, *J. Compos. Constr.* 20 (6) (2016) 04016056.
- [20] Z.C. Tetta, L.N. Koutas, D.A. Bournas, Shear strengthening of concrete members with TRM jackets: effect of shear span-to-depth ratio, material and amount of external reinforcement, *Compos. B Eng.* (2017), accepted.
- [21] D.A. Bournas, T.C. Triantafillou, K. Zygouris, F. Stavropoulos, Textile-reinforced mortar versus FRP jacketing in seismic retrofitting of RC columns with continuous or lap-spliced deformed bars, *J. Compos. Constr.* 13 (5) (2009) 360–371.
- [22] D. Bournas, T. Triantafillou, Bar buckling in RC columns confined with composite materials, *J. Compos. Constr.* 15 (3) (2010) 393–403.
- [23] D. Bournas, T. Triantafillou, Bond strength of lap-spliced bars in concrete confined with composite jackets, *J. Compos. Constr.* 15 (2) (2011) 156–167.
- [24] D.A. Bournas, T.C. Triantafillou, Biaxial bending of reinforced concrete columns strengthened with externally applied reinforcement in combination with confinement, *ACI Struct. J.* 110 (2) (2013) 193.

- [25] D.A. Bournas, A. Pavese, W. Tizani, Tensile capacity of FRP anchors in connecting FRP and TRM sheets to concrete, *Eng. Struct.* 82 (2015) 72–81.
- [26] L. Ombres, S. Verre, Structural behaviour of fabric reinforced cementitious matrix (FRCM) strengthened concrete columns under eccentric loading, *Compos. B Eng.* 75 (2015) 235–249.
- [27] L. Koutas, S. Bousias, T. Triantafillou, Seismic strengthening of masonry-infilled RC frames with TRM: experimental study, *J. Compos. Constr.* 19 (2) (2014) 04014048.
- [28] D. Bournas, Strengthening of existing structures: Selected case studies. In: T.C. Triantafillou, (Ed.), *Textile Fibre Composites in Civil Engineering* (Ch. 17): Elsevier, Woodhead Publishing Limited, 2016, 389–411.
- [29] I. Colombo, M. Colombo, A. Magri, G. Zani, M. di Prisco, Textile Reinforced Mortar at High Temperatures, *Appl. Mech. Mater.* 82 (2011) 202–207.
- [30] Silva F de Andrade, M. Butler, S. Hempel, R.D. Toledo Filho, V. Mechtcherine, Effects of elevated temperatures on the interface properties of carbon textile-reinforced concrete, *Cem. Concr. Compos.* 48 (2014) 26–34.
- [31] D.A.S. Rambo, Silva F. de Andrade, R.D. Toledo Filho, OdFM Gomes, Effect of elevated temperatures on the mechanical behavior of basalt textile reinforced refractory concrete, *Mater. Des.* 65 (2015) 24–33.
- [32] Y.A. Al-Salloum, T.H. Almusallam, H.M. Elsanadedy, R.A. Iqbal, Effect of elevated temperature environments on the residual axial capacity of RC columns strengthened with different techniques, *Constr. Build. Mater.* 115 (2016) 345–361.
- [33] S.R. Maroudas, C.C. Papanicolaou, Effect of high temperatures on the TRM-to-masonry bond, *Key Engineering Materials*, 747, Trans Tech Publications, 2017, pp. 533–541.
- [34] S.M. Raouf, D.A. Bournas, Bond between TRM versus FRP composites and concrete at high temperatures, *Compos. B Eng.* (2017), <http://dx.doi.org/10.1016/j.compositesb.2017.05.064>.
- [35] Z.C. Tetta, D.A. Bournas, TRM vs FRP jacketing in shear strengthening of concrete members subjected to high temperatures, *Compos. B Eng.* 106 (2016) 190–205.
- [36] L. Bisby, T. Stratford, C. Hart, S. Farren, Fire performance of well-anchored TRM, FRCM, and FRP flexural strengthening systems, *Adv. Compos. Constr.* (2013).
- [37] EN-12390-3. Testing Hardened Concrete-Part. 3: Compressive Strength of Test Specimens. Prague: Czech Standards Institute, 2009.
- [38] EN-12390-6. Testing hardened concrete-Tensile splitting strength of test specimens. Italian Standardization Board, 2002.
- [39] EN B. 1015-11: Methods of test for mortar for masonry-Part 11: Determination of flexural and compressive strength of hardened mortar. European Committee for Standardization, Brussels, 1999.
- [40] fib Model Code I. International Federation for Structural Concrete (fib), Vol. 1-Bulletin 55, Vol. 2-Bulletin 56. Lausanne, 2010.
- [41] fib Model Code a. Model code for concrete structures. Bulletin 14, 2010; Lausanne; Switzerland, 2010.